Chemical Abundances in Gaseous Nebulae
AAA Workshop Series 12, 2016
G. Hägele, M. Cardaci & E. Pérez-Montero, eds.

Invited Review

Chemical abundances of photoionized nebulae in the Local Group

W. J. Maciel[1], R. D. D. Costa[1] and O. Cavichia[2]

[1]*IAG, University of São Paulo, Rua do Matão 1226, 05508-090, São Paulo SP, Brazil*
[2]*IFQ, Universidade Federal de Itajubá, Av. BPS, 1303, 37500-903, Itajubá MG, Brazil*

Abstract. Photoionized nebulae comprise basically HII regions and planetary nebulae, and their abundances give important clues on the nucleosynthesis and chemical evolution of their host galaxies. There is presently a large amount of data on these objects, especially for the elements He and N, which are strongly affected by the evolution of intermediate mass stars, as well as O, Ne, S, and Ar, which are essentially synthesized in stars with larger masses. The abundances of these elements in several systems in the Local Group are discussed on the basis of distance-independent correlations.

1. Introduction

Planetary nebulae (PN) provide accurate abundances of elements that are not significantly produced by their progenitor stars such as O, Ne, S, and Ar, as well as some elements for which the abundances have been changed, such as He, N, and C. The former can be used to study the chemical evolution of the host galaxies, and the latter can place constraints on the nucleosynthesis of intermediate mass stars. Distance-independent correlations involving O, Ne, S, and Ar can then be compared with the corresponding abundances of young objects, such as HII regions, Blue Compact Galaxies (BCG) and Emission Line Galaxies (ELG). In this paper we intend (i) to compare the abundances of HII regions and PN in different galaxies of the Local Group in order to investigate the differences derived from the age and origin of these objects, (ii) compare the chemical evolution in these systems, and (iii) investigate to what extent the nucleosynthesis contributions from the progenitor stars affect the observed abundances in planetary nebulae. Section 2 describes the data used in this investigation, and Section 3 presents our results and discussion. Further details can be found in Maciel et al. (2017).

2. The Data

We have considered abundance data for PN and HII regions in the following objects: The Milky Way (MW), the Large Magellanic Cloud (LMC), the Small

Magellanic Cloud (SMC), M31, M32, M33, M51, M81, M101, NGC 185, NGC 205, NGC 300, NGC 628, NGC 3109, NGC 5194, and the Sextans galaxy. The uncertainties are typically of 0.2 to 0.3 dex for PN and 0.1 to 0.2 dex for HII regions. The PN sample includes over 1300 objects, while the HII region sample has over 900 objects, as shown in Table 1. We have preferably used the PN data obtained by our own group, but have also considered some recent abundance determinations from the literature, particularly from sources using a similar procedure as our group. For HII regions we have preferably adopted abundances obtained from detailed electron temperatures, instead of the strong line method. Blue Compact Galaxies and Emission Line Galaxies have also been included, as they are essentially low metallicity HII regions. The samples are large enough to compensate for the inhomogeneity of data, as a large number of sources has to be considered, since there is no complete homogeneous sample available. The complete list of sources for each object is given by Maciel et al. (2017).

Table 1. Total samples.

Planetary Nebulae	Number	HII Regions	Number
Milky Way Disk	347	Milky Way	216
Milky Way Bulge	267	Magellanic Clouds	35
Milky Way	614	Other Galaxies	325
Magellanic Clouds	511	BCG, ELG	360
Total External Galaxies	704	Total External Galaxies	720
TOTAL	1318	TOTAL	936

3. Results and Discussion

3.1. O, Ne, S, and Ar

Figure 1 shows histograms of the oxygen abundance O/H for planetary nebulae and HII regions in two representative cases: The Milky Way (left panels) and all objects considered here, namely the Milky Way, the Magellanic Clouds and the remaining external galaxies (right panels). Both PN and HII regions have similar distributions, although the HII region distributions are generally broader than in the case of planetary nebulae. Also, it can be noticed that a larger fraction of HII regions have $\log(\mathrm{O/H}) + 12 \geq 9$, which reflects the fact that these younger objects are formed by more enriched material. Similar plots can be obtained for Ne, S, and Ar.

Distance-independent correlations for Ne are shown in Figure 2. The left panels refer to the Milky Way, while the right panels are for all objects considered. The top figures show the abundances relative to hydrogen (Ne/H), while the bottom figures show the abundances relative to oxygen (Ne/O). The squares represent Milky Way PN, the circles are external PN, the triangles represent HII regions in the Milky Way, and the crosses are external HII regions. We see that for the Ne/H ratio both PN and HII regions present a lockstep variation with O/H, although for HII regions the dispersion is much smaller. This is also reflected in

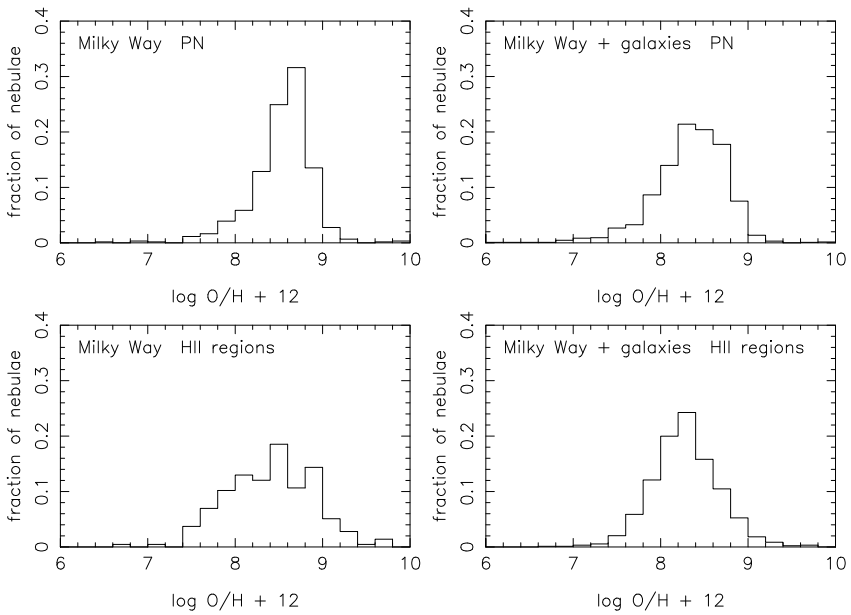

Figure 1. Histograms of the O/H abundances in PN and HII regions. Left: Milky Way; Right: Milky Way and external galaxies.

the bottom figure, indicating that the Ne/O ratio is essentially constant with a higher dispersion for PN. The estimated dispersions are about 0.2 dex for PN and 0.1 dex for HII regions.

The same behaviour observed in the Galaxy also holds in other Local Group objects. Despite their different metallicities and morphologies, their nucleosynthetic processes and chemical evolution are apparently very similar. The trend displayed in Figure 2 (right) shows a very good agreement with the trend found by Izotov et al. 2006 on the basis of ELG only. Similar conclusions were obtained by Richer and McCall 2007, 2008. For the right panel, the fractions of objects within 1σ and 2σ are 0.78 and 0.93, respectively.

It is interesting to notice that in this larger sample the observed ranges of oxygen and neon abundances in PN and HII regions are similar. The similarity essentially reflects the fact that the interstellar metallicities did not change appreciably in the last 5 Gyr approximately, a result that is supported by determinations of the age-metallicity in the Milky Way (see for example Rocha-Pinto et al. 2000, Bensby et al. 2004.

The results shown in Figure 2 can be interpreted assuming that the dispersion in the PN data reflects the fact that the abundances are not as well determined as in the HII regions. However, a larger dispersion would be expected, since PN are older objects than the HII regions and any given sample probably includes objects of different ages, as we have shown elsewhere (Maciel et al. 2010, 2011). It can also be considered that there is some contribution to the Ne abundances from the PN progenitor stars, as suggested in some investigations (see for example Peña et al. 2007). It has been argued that the third dredge-up process in AGB

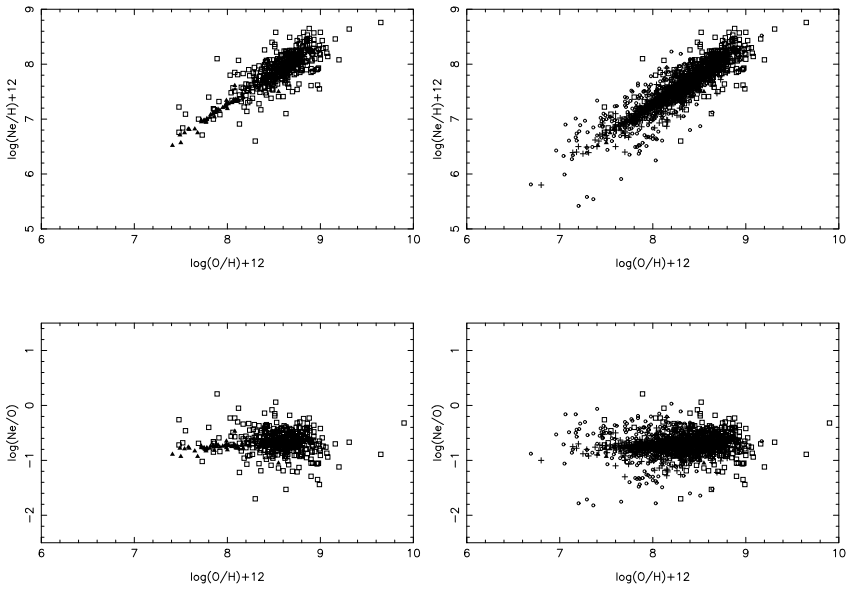

Figure 2. Ne abundances as functions of oxygen abundances. Left: Milky Way, right: Milky Way and external galaxies. Milky Way PN (squares), Milky Way HII regions (triangles); external PN: circles, external HII regions: crosses

stars may affect the oxygen abundances observed in PN (see for example Karakas & Lattanzio 2014). ON cycling would also reduce the O/H ratio especially in lower metallicity PN with massive progenitor stars (see for example Karakas & Lattanzio 2007). Our results show that, if present, such contribution should be small compared with the average uncertainties in the PN abundances, so that an average contribution of about 0.1 dex cannot be ruled out. On the other hand, if we compare the expected contributions both to oxygen and neon, it is unlikely that their are equal, which is needed in order to explain the similarity of the PN and HII region trends shown in Figures 2 (cf. Karakas and Lattanzio 2003).

In the case of sulphur, as shown in Figure 3, the general trends with oxygen are similar to neon, but some differences arise. The average dispersions are now 0.3 dex for PN and 0.2 dex for HII regions. For the Milky Way, the HII regions present a very good correlation, and the data extend to higher and lower metallicities compared with neon. The galactic PN already display what is usually called the "sulphur anomaly", that is, many PN apparently have somewhat lower S/H abundances than expected for their metallicity (see the detailed discussions by Henry et al. 2004, 2012). The sulphur anomaly has been attributed to a deficiency in the sulphur ICFs, particularly due to the abundance of the S^{+3} ion, lack of accurate atomic constants, effect of the nucleosynthesis in the progenitor stars, and different chemical evolution of the systems considered.
Considering the right panel of Figure 3, it can be seen that there is still a reasonable number of objects below the HII region curve, but there is a large number of PN in the opposite side, so that the sulphur anomaly is not particularly notice-

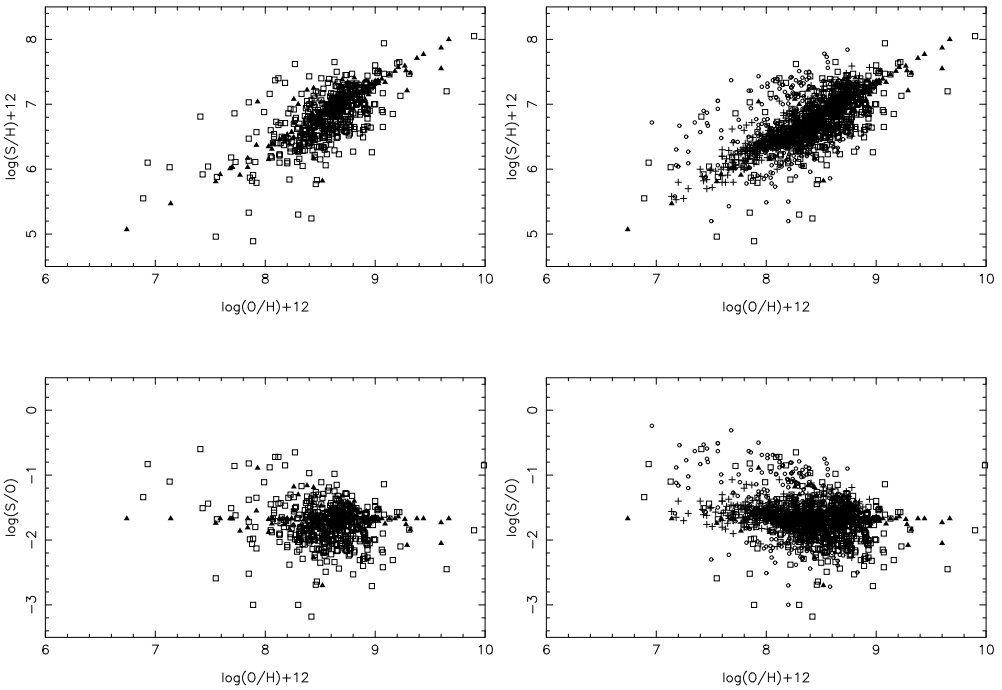

Figure 3. The same as Figure 2 for Sulphur

able. The inclusion of BCG and ELG maintains these conclusions, that is, the sulphur abundances of HII regions apparently do not show the sulphur anomaly, which is then a characteristic of the empirical determination of sulphur abundances in PN.

For argon the observed correlations are similar compared to neon, but the dispersion is higher and is comparable to S/H, as can be seen from Figure 4. The comparison with HII regions suffers from the lack of data for this element, especially for the Milky Way. The inclusion of BCG and ELG clearly improves the correlation, showing that the correlation defined at higher metallicities for the Milky Way still holds for lower and intermediate oxygen abundances. For PN, the Ar/H dispersion is higher compared with Ne/H, but for HII regions the dispersions in Ne/H, S/H, and Ar/H for the whole sample are similar to each other, and always smaller than the PN data. Therefore, the HII regions are clearly more homogeneous than the PN, which reflects their very low ages, roughly a few million years.

3.2. Elements produced by the PN progenitor stars

Histograms of the N/H abundances for PN and HII regions in our sample are shown in Figure 5, which can be directly compared with Figure 1. The PN distribution is similar in the two cases shown, while for HII regions the inclusion of external galaxies (as well as BCG and ELG) shifts the maximum downwards by about 0.5 dex. The main difference between O/H and N/H is that the nitrogen

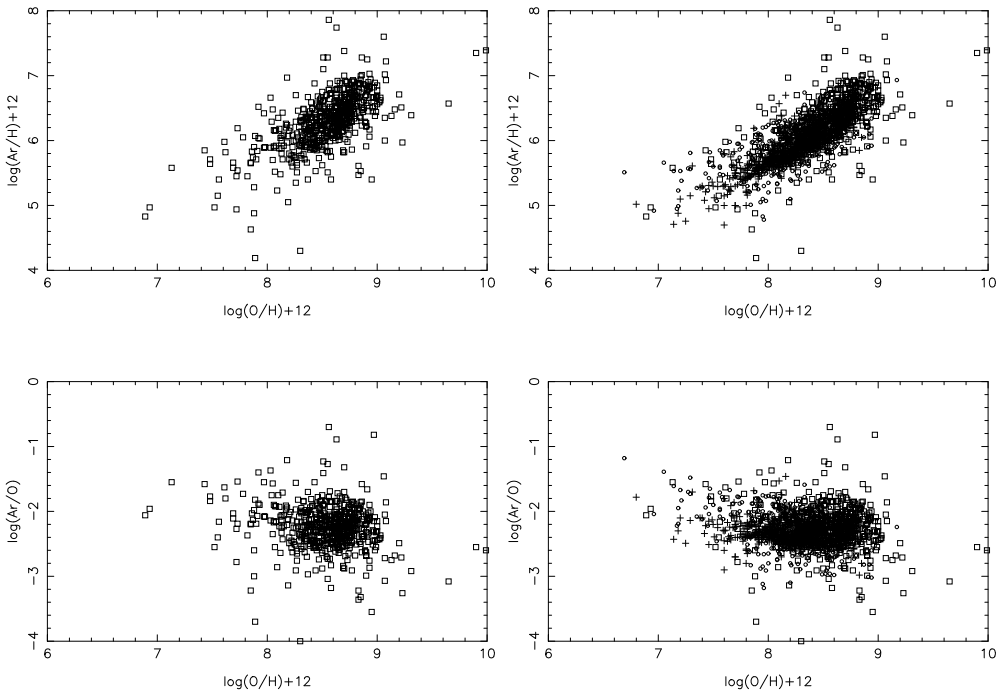

Figure 4. The same as Figure 2 for Argon

abundances extends to lower metallicities for HII regions compared with PN, which reflects the N production during the evolution of the PN progenitor stars.

Helium abundances in HII regions are frequently affected by the presence of neutral helium, so that in this work we have adopted a lower limit of He/H = 0.03 in order to avoid objects with an important fraction of neutral He.

Figure 6 shows the N/H and N/O ratios as functions of O/H and He/H, respectively, for the case where all objects are considered. The most striking result is that, as expected, PN show an increase in both N and He compared to most HII regions in the sample. The average dispersions of the nitrogen data are higher, about 0.4 dex for PN and 0.3 dex for HII regions. Therefore, a larger dispersion is also observed for HII regions, so that part of their nitrogen is probably secondary.

Our results clearly reflect the fact that the nitrogen abundances measured in PN include both the pristine nitrogen plus the contribution from the dredge up processes that affect the red giant progenitor stars. Similar trends have also been recently discussed by García-Hernández et al. 2016. Adopting a pregalactic He abundance by mass of about $Y = 0.255$ (cf. Izotov et al. 2014), which corresponds to approximately He/H = 0.09, we conclude from Figure 6 (bottom) that about 80% of the PN with He excess have abundances up to He/H $\simeq$ 0.141, which is about 57% higher than the pregalactic value. This can be compared with an amount of 50% derived by Richer & McCall 2008 from a smaller sample. More recently, Lattanzio & Karakas 2016 suggested an increase of about 38% in the helium content by mass from the second dredge-up process in AGB stars,

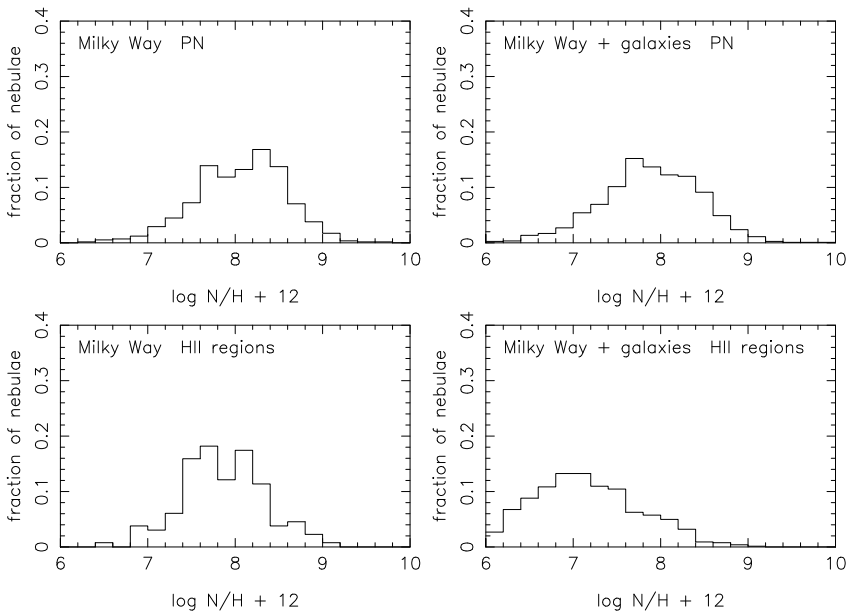

Figure 5. Histograms of the N/H abundances in PN and HII regions. Left: Milky Way, Right: Milky Way and all external galaxies.

which would lead to an increase of about 60% in the He abundance by number of atoms, in excellent agreement with the results shown in Figure 6.
Also from Figure 6 we can have an idea of the amount of nitrogen produced by the progenitor stars. Adopting as limit for primary nitrogen the amount produced by type II supernovae (Izotov et al. 2006), corresponding to approximately $\log \mathrm{N/O} = -1.6$, and considering the expected secondary nitrogen enrichment, which corresponds to about $\log \mathrm{N/O} = -1.2$, Figure 6 (bottom) implies that about 80% of the PN present an enrichment ratio up to factor of 13.3, comparable with the factor of 10 found by Richer & McCall (2016).
In Figure 6 (bottom) we include a comparison with some recent theoretical models by Karakas 2010 with $Z = 0.02$, 0.004, and 0.008, while the dashed lines represent models by Marigo et al. 2003 with $Z = 0.019$. According to these models, progenitors having 0.9 to 4 $M_{\odot}$ and solar composition can explain the "normal" abundances, $\mathrm{He/H} < 0.15$, while for objects with higher enhancements ($\mathrm{He/H} > 0.15$), masses of 4 to 5 $M_{\odot}$ are needed, plus an efficient HBB. Recent models by Pignatari et al. 2016 with $Z = 0.01$ and 0.02 are also consistent with these results, as can be seen in the discussion by Delgado-Inglada et al. 2015. For intermediate mass stars, agreement with theoretical models is fair, but abundance determinations should be improved and expanded.

Acknowledgments. This work was partially supported by FAPESP, CNPq, and CAPES.

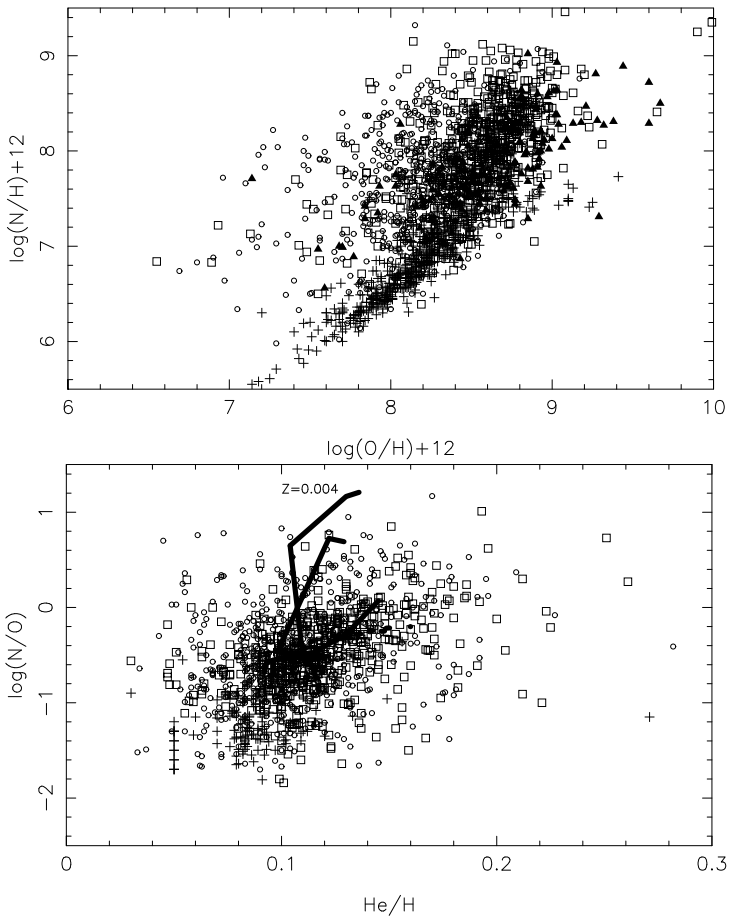

Figure 6. N abundances as functions of O/H (top) and He/H (bottom) for the Milky Way and external galaxies. MW PN (squares), MW HII regions (triangles), external PN (circles), external HII regions (crosses). The lines are models by Karakas (solid lines) and Marigo (dashed line).

References

Bensby, T., Feltzing, S., Lundström, I. 2004, A&A 421, 969

Delgado-Inglada, G., Rodríguez, M., Peimbert, M., Stasińska, G., Morisset, C. 2015, MNRAS 449, 1797

García Hernández, D. A., Ventura, P., Delgado-Inglada, G., DellŠAgli, F., Di Criscienzo, M., Yagüe, A. 2016, MNRAS 461, 542

Henry, R. B. C., Kwitter, K. B., Balick, B. 2004, AJ 127, 2284

Henry, R. B. C., Speck, A., Karakas, A., Ferland, G. I., Maguire, M. 2012, ApJ 749, 61

Izotov, Y. I., Stasińska, G., Meynet, G., Guseva, N. G., Thuan, T. X., 2006, A&A 448, 955

Izotov, Y. I, Thuan, T. X., Guseva, N. G. 2014, MNRAS 445, 778

Karakas, A. 2010, MNRAS 403, 1413

Karakas, A.. Lattanzio, J. C. 2003, PASA 20, 293

Karakas, A., Lattanzio, J. C. 2007, PASA 24, 103

Karakas, A.. Lattanzio, J. C. 2014, PASA 31, 30

Lattanzio, J., Karakas, A. 2016, Journal of Phys. Conf. Ser. 728, 022002

Maciel W. J., Costa, R. D. D., Cavichia. O. 2017, Rev. Mex. Astron. Astrof. (submitted)

Maciel, W. J., Costa, R. D. D., Idiart, T. E. P. 2010, A&A 512, A19

Maciel, W. J., Rodrigues, T. S., Costa, R. D. D. 2011, RMAA 47, 401

Marigo, P., Bernard-Salas, J., Pottasch, S. R., Tielens, A. G. G. M., Wesselius, P. R. 2003, A&A 409, 619

Peña, M., Stasińska, G., Richer, M. G. 2007, A&A 476, 745

Pignatari, M., Herwig, F., Hirschi, R., et al. 2016, ApJS 225, 24

Richer, M. G., McCall, M. L. 2007, ApJ 658, 328

Richer, M. G., McCall, M. L. 2008, ApJ 684, 1190

Richer, M. G., McCall, M. L. 2016, Focus Meeting 4, XXIX IAU General Assembly, ed. P. Benvenuti (arXiv:1509.08537)

Rocha-PInto, H. J., Maciel, W. J., Scalo, J., Flynn, C. 2000, A&A 358, 850